Biosensors and Bioelectronics 135 (2019) 14–21

Contents lists available at ScienceDirect

Biosensors and Bioelectronics

journal homepage: www.elsevier.com/locate/bios

Phosphorene-gold nanocomposite based microfluidic aptasensor for the detection of okadaic acid

Saipriya Ramalingam[a], Rohit Chand[b], Chandra B. Singh[c], Ashutosh Singh[a,*]

[a] School of Engineering, University of Guelph, Guelph, ON, N1G 2W1, Canada
[b] W. Booth School of Engineering Practice and Technology, McMaster University, Hamilton, ON, L8S 4L8, Canada
[c] Stored Grains Engineering, School of Engineering, University of South Australia, Adelaide, SA, 5001, Australia

ARTICLE INFO

Keywords:
Okadaic acid
Phosphorene
Phosphorene-gold
2D nanomaterials
Microfluidics

ABSTRACT

Okadaic acid (OA) is one of the most prevalent and largely distributed bio-toxin in the world. Consumption of OA results in a series of digestive ailments such as nausea and diarrhea. This study demonstrates the preparation and functioning of an electrochemical microfluidic biochip for the detection of OA. The screen-printed carbon electrode (SPCE) was modified by phosphorene-gold nanocomposite onto which an aptamer specific to OA was immobilized. BP-Au nanocomposites were synthesized by an in-situ, one-step method without the use of a reducing agent. Potassium ferro-ferri cyanide was used as a redox pair to quantify signal strength. To improve reaction time, increase sensitivity and portability, a microfluidic platform was designed and developed. This device comprised of channels identified for specific purposes such as sample mixing and incubation. Overall, the integrated system consisted of a polydimethylsiloxane microfluidic chip housing an aptamer modified SPCE, as a single detection module for Okadaic acid. The nanomaterials and the microfluidic channels prepared were spectroscopically and electrochemically analyzed. Differential pulse voltammograms revealed a detection limit of 8 pM, while a linear range was found between 10 nM–250 nM. Selectivity studies were also performed with spiked mussel samples and other interfering species. This point-of-care device can be deployed to perform on-farm assays in fishing units.

1. Introduction

Photosynthetic organisms (marine algal blooms) often flourish during the warm summer months of the year. However, some phytoplankton, broadly classified under “harmful algal blooms” (HABs), produce chemically stable compounds which negatively impact human health (Hallegraeff, 1993). With shifting global dynamics, it has been hypothesized that environmental changes and climatic fluctuations increase the production of HABs (Landsberg, 2002). A by-product of HAB is Okadaic Acid (OA), which originates from algal genera *Prorocentrum* and *Dynophysis*. The okadaic acid group of biotoxins, consist of okadaic acid (OA) and its analogues dinophysistoxins 1, 2 and 3 (DTX-1, DTX-2 and DTX-3) (Morabito et al., 2018). Chemically, OA [$C_{45}H_{68}O_{13}$] is a polyether fatty acid derivative and has been recognized as a major toxic compound in Diarrheic Shellfish Poisoning (DSP). OA accumulates widely in the adipose tissue of bivalve marine species such as clams, mussels, and scallops. Ingestion of OA contaminated seafood, results in a series of gastrointestinal symptoms like vomiting, diarrhea, abdominal cramps, collectively known as DSP (Ishihara et al., 1989). OA poisoning occurs by the inhibition of major Ser/Thr protein phosphatases – PP1, PP2A and PP2C. These phosphatases (enzymes) control cellular phosphorylation and de-phosphorylation activities which help maintain the cytoskeletal structural and functional integrity. In addition, OA is also a potent tumor promoter, known to initiate the TNF-α pathway causing tumors in different parts of the body Haystead et al. (1989); Cohen et al. (1990). Hence, the buildup of these biotoxins in marine life has raised food safety concerns among fishing industries and governments worldwide.

According to European standards (CE No: 853/2004) the maximum threshold level for OA in sea-food are set at 160 μg/kg (of shellfish meat) (“European Food Safety Authority,” 2008). This low permissible limit has urged scientists and researchers to look for effective detection techniques. Various analytical methods have been developed over the years, the first of which was the mouse bioassay (MBA). This in-vivo assay was considered the standard method for the quantification of OA until 2011 (EC No.15/2011). Although it is the simplest screening method, MBA caused large variability in results due to mouse gender, health and low specificity to toxins (Suzuki and Okada, 2018).

* Corresponding author.
E-mail address: asingh47@uoguelph.ca (A. Singh).

https://doi.org/10.1016/j.bios.2019.03.056
Received 15 January 2019; Received in revised form 21 March 2019; Accepted 26 March 2019
Available online 05 April 2019
0956-5663/

Advancements in science and technology gave rise to lab-based techniques which alleviated costly animal maintenance and ethical issues. Chromatographic techniques such as Capillary Electrophoresis (CE) (de la Iglesia et al., 2007) and liquid chromatography mass-spectroscopy (LCMS) were introduced, which gave a limit of detection of ~0.015 μg/g (Suzuki et al., 2009). The LCMS was later recognized as the standard technique for OA detection due to good sensitivity, repeatability, and insight into structural information (Sassolas et al., 2013). A combination of micellar electrokinetic chromatography and ultraviolet detection was used to determine the concentration of Okadaic acid in a sample by (Bouaïcha et al., 1997) with a linear range of 40–640 pg/ml. In the last decade, immunological detection methods gained popularity owing to their sensitivity, cost-effectiveness and high recovery. Direct and competitive Enzyme-linked Immunosorbent Assay (ELISA) were designed on the basis of simple antigen-antibody interaction. Variable parameters for any immunological sensing system are (a) Mode of Ab immobilization (b) choice of the transducer and (c) surface modification (Stewart et al., 2009). Based o these considerations, several immunosensing platforms were developed namely: electrochemical, piezoelectric, optical, surface plasmon resonance (SPR) and chemiluminescence (Su et al., 2017). Among the above listed various sensing techniques, electrochemical sensing has garnered attention due to its selectivity, analyte specificity, and easy handling. However, drawbacks include longer analysis time, multiple washing steps and cost of antibodies.

With the development in molecular sciences, nanomaterials were discovered to have enhanced properties as compared to their bulk counterparts. The 2D nanomaterials (2DM) were preferred as they possess a unique sheet-like ultrathin structure of a few atomic layers (Zhang et al., 2018). Their simple preparation, easy functionalization, and biocompatibility made 2DM a promising transducer modification for improved biosensor performance. Further, challenges faced by immunosensor technology gave rise to the discovery of aptamers which are short DNA strands, approximately 25 bases long. The Systematic Evolution of Ligands by Experimental Enrichment (SELEX) process is employed to screen large combinations of DNA libraries and the sequence having an affinity to target is isolated on the basis of its dissociation constant (K_d) (Wu and Kwon, 2016). Some of the advantages aptamers have over antibodies include: (1) better shelf life and stability, (2) can be made synthetically and does not require an animal source, (3) kinetic parameters can be altered according to application, (4) minimal batch to batch variation, and (5) high specificity (Teller et al., 2009).

Herein, a unified aptasensing system for the detection of OA was developed taking into account the positives of 2DM nanocomposites. Phosphorene nanosheets have been chosen for the purposes of this research, as they have proven to be a good alternative to graphene (Ahmed et al., 2017). Black Phosphorous (BP) is known for stability, unique hinge structure, high band gap and reactive edge structure (Ren et al., 2017). A high bandgap activity of 0.36eV has been observed by (Liu et al., 2014) indicating high hole mobility in exfoliated BP sheets. Further, its property to reduce bulk gold into nanoparticles without the use of a reducing agent, like sodium citrate has been validated in this paper. The working of the electrochemical sensor was enhanced by incorporating multiple layers of BP-Au NC. The synthesized BP-Au NC served as a backbone to the aptamer sequence, fastening it throughout the process. The use of a ferro-ferri cyanide redox probe eases the sensing process, thus yielding a label-free electrochemical sensor. The interaction of OA specific aptamer with target causes a variation in charge transfer on the surface of the electrode. A higher concentration of OA would lead to reduced current output while the reverse would happen at lower concentrations. In addition, this paper also highlights the fabrication of a microfluidic biochip for OA detection. This integrated chip comprises of specific zones for on-chip functions such as incubation, mixing and sensing. The nanomaterials synthesized were characterized using Transmission electron microscopy, Raman Spectroscopy, Energy Dispersive X-Ray Analysis (EDX) and UV- Visible spectroscopy in addition to electrochemical studies such as Cyclic Voltammetry (CV) and Differential Pulse Voltammetry (DPV).

2. Experimental procedure

2.1. Materials

Black phosphorous powder was obtained from ACS Materials (CA, USA). Hydrogen tetrachloroaurate (III) hydrate ($HAuCl_4$. $3H_2O$), potassium hexacyanoferrite (K_3 $[Fe(CN)_6]$), potassium hexacyanoferrate (K_4 $[Fe(CN)_6]$), phosphate buffer saline (PBS) tablets, N-methyl-2-pyrrolidone (NMP) and Lysozyme (chicken egg white) were purchased from Millipore Sigma (Oakville, ON, Canada). Milli- Q water (18.2 MΩ, DI water) was used throughout the experiment and fresh buffers were prepared whenever required. Carbon screen-printed electrodes (SPCE) were obtained from Orion High Technologies (Spain). The SPCE has a working electrode of 4 mm diameter, an (Ag/AgCl) reference electrode and a carbon counter electrode on a flexible PET substrate. For the preparation of microfluidic chips, PDMS (Sylgard, 184), an elastomer base and curing agent were obtained from Dow Corning (Canada). SU-8 Photoresists (SU-8 2025) and developer were purchased from MicroChem Corp. (Westborough, MA, USA). Okadaic acid sodium salt and Brevetoxin were acquired from Abcam (Canada). Aptamer sequences specific to Okadaic acid were determined from previous studies (Eissa et al., 2013; Wu et al., 2015) and synthesized by IDT Technologies (USA). The aptamer (OA- Apt) sequence chosen is as follows:

5′- Thiol -GGTCACCAAC AACAGGGAGC GCTACGCGAA GGGTCAA TGT GACGTCATGC GGATGTGTGG-3'.

The 5′ end of the aptamer was thiolated (-SH) so that it can readily bind with the synthesized BP-Au nanocomposite. TE buffer (10 mM Tris/1 mM EDTA) was used to re-suspend the lyophilized aptamer to yield a stock solution of 100 μM.

2.2. Nanocomposite synthesis and characterization

The BP-Au nanocomposite preparation was based on the in-situ reduction capacity of BP nanosheets on $HAuCl_4$. In brief, 20 mg BP crystals were dispersed in 20 ml of NMP and exfoliated for a period of 8 h (Fig. S1). The sonication tip was set to a power of 200 W with a 2 s ON time and a 4 s OFF time. The mixture was immersed in an ice bath to maintain the temperature around 5 °C throughout the process. Further, the dispersion was centrifuged at 5000 rpm for 10 min to obtain BP nanosheets. BP-Au nanocomposite (BP-Au NC) was prepared by the addition of 5 ml of BP stock solution to 20 ml of boiling water. To this dispersion, 20 mM of $HAuCl_4$ was added and allowed to boil for a period of 2 min. A change from blackish-yellow to a deep purple color marked the formation of BP-Au NC. Further, the mixture was taken off the heat and allowed to stir at room temperature for a period of 2 h. Once cooled, BP- Au NC was stored in the refrigerator at 4 °C for later use.

Characterization of the synthesized BP and BP- Au NC was done using UV- VIS Spectrophotometer (DR- 6000 UV-VIS, Hach, Germany), Transmission Electron Microscopy (TEM, Tecnai G2 F20,USA), Raman Spectroscopy (Renishaw inVia Raman Microscope) and EDX Energy Dispersive X-Ray Spectroscopy (FEI Inspect S50, SEM, USA).

2.3. Electrode modification

Bare screen-printed carbon electrodes (SPCE) were first characterized for their current characteristics before modification. The CV studies were performed in the presence of 5 mM $[Fe(CN)_6]^{3-/4}$ redox indicator. Working electrodes were modified by drop casting 10 μL of the synthesized BP-Au NC dispersion on the working electrode. Following that, the electrodes were oven dried at 40 °C to promote adhesion to the surface. Multiple layers of BP-Au NC were drop-cast, to ensure an even

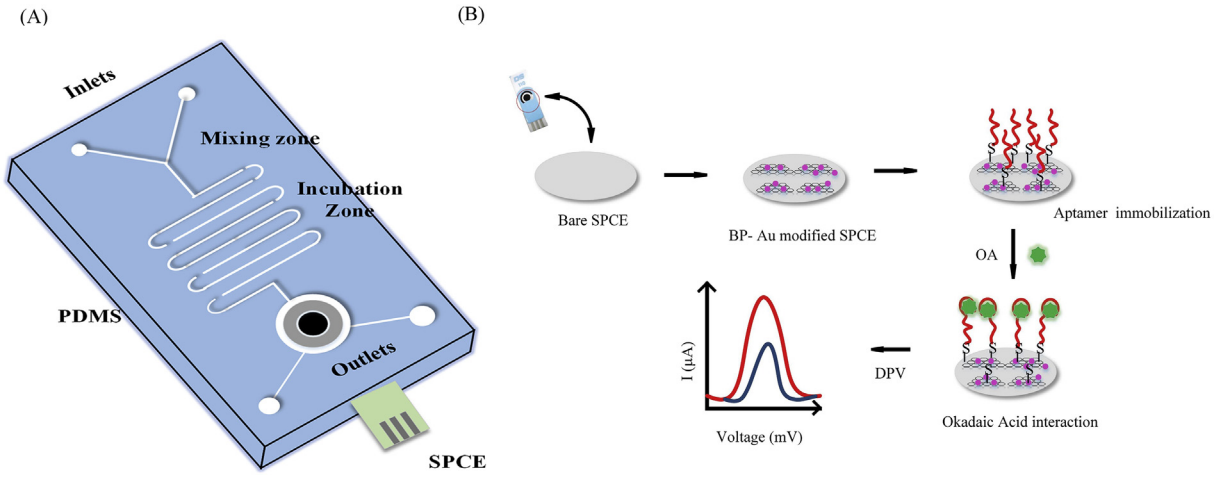

Fig. 1. Microfluidic electrochemical aptasensor for the detection of Okadaic Acid: (A) Graphical of the fabricated PDMS microfluidic chip (B) Schematic representation of the process of aptamer-based sensing.

coat of nanocomposite on the surface. These SPCEs were further functionalized by immobilizing the aptamer specific to Okadaic acid (Fig. 1B). Various aptamer concentrations ranging from 0.25 μM–2 μM were drop-cast onto the functionalized electrodes and incubated overnight in a moisture chamber at 6 °C. At the end of the binding process, the electrodes were gently washed using DI water to remove unbound aptamers. The prepared electrodes were stored at 4 °C for later use.

2.4. Microfluidic device design

A soft lithographic technique was used to fabricate a flexible PDMS microfluidic chip. Fig. 1(A) is a graphical representation of the fabricated Y- channel microfluidic device comprising of two inlets, an incubation channel, a sensing zone, and outlets. The microfluidic channel was first designed using AutoCAD® software, which was developed into the desired photomask (CAD/Art Services, Inc., OR, USA). Next, SU-8 negative photoresist was carefully spin coated (Brewer Science, USA) on the surface of a clean silicon wafer. The modified silicon wafer was baked for a stipulated time period to improve adhesion between the resist and the substrate. This step was followed by exposing the substrate to UV light (UV- KUB2) through the photomask to develop the required pattern. Post-exposure baking and SU-8 development were done to obtain the final master mold. Meanwhile, a mixture of Sylgard 184 PDMS and its curing agent, in the ratio 10:1 was mixed vigorously and degassed. This mixture was carefully poured over the master mold and cured for a period of 3 h at 75 °C in a hot air oven. At the end of the curing period, the PDMS replica of the mold was peeled off and holes for inlet and outlet were punched.

The bottom layer was prepared by pouring a thin layer of PDMS onto a mold containing a chamber matching the dimensions of the SPCE. The PDMS obtained was cut in accordance with previously prepared channel bearing layer. OA-Apt functionalized SPCE was precisely glued onto the groove of the bottom layer. Following this, both layers were treated with oxygen plasma (Harrick Plasma, PDC-32G, USA) for 30 s. The top and the bottom layers were carefully aligned and bonded, with the help of a light microscope. Care was taken to ensure no leakage occurred between the layers.

2.5. Electrochemical detection of OA

The fundamental working principle of this sensor is based on the interaction between OA specific aptamer sequence and the incoming target. A change in overall resistance is observed when the OA- Apt sequence (attached to BP-Au NC) captures the OA in solution. In order to determine the interaction time required between OA and OA- Apt, various intervals ranging from 5 to 60 min were studied. Okadaic acid stock solution (1 mM) was prepared in 1 mM TE buffer (pH 7.0). Different concentrations of OA targets were injected manually into the sensing zone and allowed to interact at room temperature.

The performance of the aptasensor for OA was tested with the help of PalmSens® (PalmSens4, Netherlands) electrochemical interface. Electrochemical parameters such as Cyclic Voltammetry (CV) and Differential Pulse Voltammetry (DPV) were explored. A solution of 5 mM $[Fe(CN)_6]^{3-/4-}$ in 1 ml TE buffer was used as a redox pair for the experiment. CV measurements were recorded in the range −0.5 V to 0.8 V with a scan rate of 20 mV/s. The OA- OA Apt binding studies were performed using DPV in the scan range −0.2–0.5 V at a scan rate of 25 mV/s and amplitude of 50 mV. A step potential of 2 mV and a current range of 1 μA was set for all DPV studies. The microfluidic chip integrated with the modified SPCE was connected to the potentiostat for electrochemical measurements.

2.6. Real sample preparation

Fresh mussels were purchased from the local market and its tissue was separated from the shell. The mussel tissue mass was run under DI water and the excess fluid was strained off using absorbent towels. The extraction process was adapted from (Weng and Neethirajan, 2018) wherein briefly, 250 mg of mussel tissue was homogenized with the help of a laboratory blender to make a smooth paste. To this, 1 ml of 50% methanol was added and mixed for 5 min. The methanolic extract was later subject to centrifugation at 4000 rpm for 5 min. The supernatant was isolated into a fresh centrifuge tube and flash heated for 5 min at 80 °C and centrifuged at 5000 rpm for 7 min. Again, 100 μL of this supernatant was suspended in TE buffer and stored at 4 °C for further experimentation (Fig. S5).

3. Results and discussion

3.1. BP-Au NC synthesis and SPCE modification

The BP nanosheets were synthesized using a facile liquid exfoliation technique of bulk phosphorene crystals. The structural and functional properties of phosphorene were analyzed using various characterization techniques. Elemental analysis (EDX) on exfoliated phosphorene and phosphorene gold nanocomposite were performed to understand the distribution of AuNP on the surface of BP (Fig.S2(A)). The presence of phosphorous, carbon and oxygen in the synthesized nanosheets proves the formation of BP. Morphological characteristics of BP nanosheets were further explored using TEM where a dispersion of BP

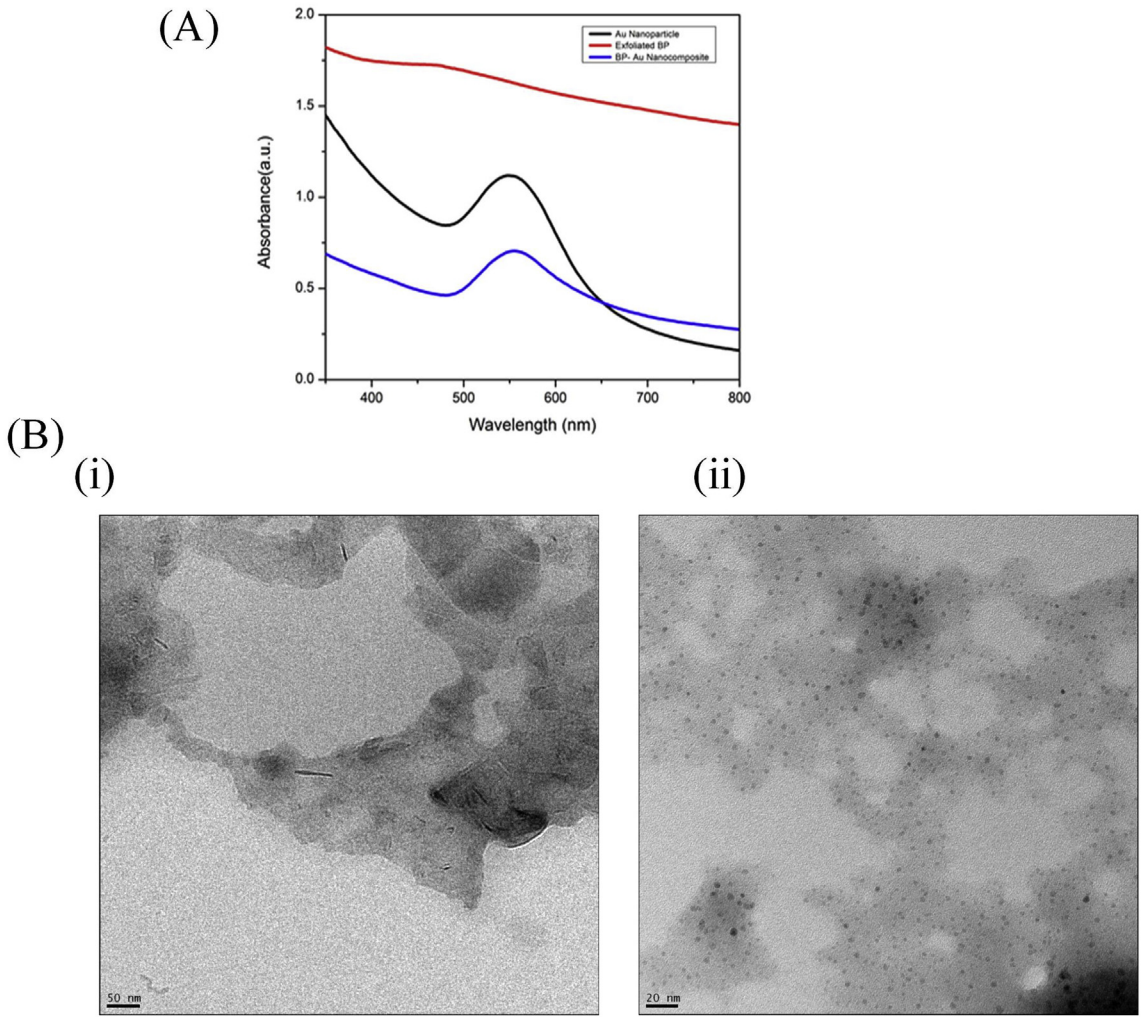

Fig. 2. Structural Characteristics of BP-Au NC: (A) UV-Vis Spectra of BP, BP- Au and Au Nanoparticles (B) TEM image of (i) BP sheets and (ii) BP-Au Nanocomposites.

nanosheets (1 mg/ml) was briefly sonicated drop-cast onto a mesh grid and air dried (Fig. 2B(i)). The TEM studies revealed that the BP nanosheets had a typical layered structure and sheet-like pattern. Interlayer interactions between BP sheets are governed by weak van der Waals forces and strong in-plane bonds (Stanford et al., 2018). These properties lead to stacking-up of a few layers to form one of the most stable 2D materials. The synthesis of BP- Au nanocomposites was performed by an in-situ, single step method without the presence of a reducing agent. Citrate reduction is ideally used for the reduction of gold salt into Au nanoparticles. It was identified that, when Au salt was introduced into a boiling solution of phosphorene in DI water, the solution turned purple within 4 min. This observation validated the reducing nature of BP in an aqueous medium and further confirmation was obtained using microscopic studies. TEM of BP-Au NCs confirmed the attachment of Au nanoparticles to the surface of phosphorene sheets. A higher magnification was employed to understand the surface morphology of the nanocomposite. A larger population of Au nanoparticles were observed around the edges of the BP nanosheets. This could be due to sheet-like structure of BP and $AuCl_4$-attaching itself to the corners as a starting point for further nucleation (Shi et al., 2013). The size of the Au nanoparticles (Fig. 2B(ii)) was calculated using ImageJ and was averaged to be ~6 nm. This finding can be attributed to the fact that the addition of water during BP-Au synthesis plays a significant role in the degradation of BP and hence the growth of Au on its surface (Huang et al., 2017). The UV-VIS spectroscopic analysis was performed on BP nanosheets, BP-Au NC and prepared Au nanoparticles. A wide excitation band observed in the UV- NIR region is responsible for a light yellowish color to the prepared BP nanosheets. A strong absorbance band was observed due to surface plasmon resonance by the Au nanoparticles around 550 nm (Fig. 2A). The BP-Au NCs UV-VIS spectra also exhibited the characteristic gold peak conforming the formation of the composite. The Raman spectra of phosphorene nanosheets gave an insight to its Raman active modes. As shown in (Fig. S2 (B)), A_g^2 and B_g^2 in-plane modes were observed at 467 cm^{-1} and 439 cm^{-1} respectively. Out -of- plane modes (A_g^1) vibrational mode was observed at 362 cm^{-1}. In the case of B_g^2 vibrational mode, the phosphorous atoms vibrate in the arm-chair plane, while in the A_g^2 mode they vibrate along the zig-zag direction (Wu et al., 2018). The BP-Au NCs however, exhibited a slight red shift which could be due to the influence of Au nanoparticles. The observed results were in tandem with previously established studies (Yang et al., 2017).

The working electrode of the SPCE was modified with BP-AuNCs and its performance as a biosensor was evaluated. Pristine carbon electrodes were subject to CV where 5 mM $[Fe(CN)_6]^{3-/4-}$ was used as a redox couple. The inert nature of carbon did not contribute to any unique response in peak current. On the other hand, electrode modification with BP-AuNC provided a significant change in anodic and cathodic peak current. The cyclic voltammograms of electrode modifications are illustrated in (Fig. S3(A)). Maximum peak current was observed in BP-Au NC modified electrodes while the same greatly reduced when OA target interacted with OA Apt on the electrode surface. The BP-Au NC peak current characteristics were in accordance to the

structural characteristics of BP-AuNC. BP nanosheets are known to exhibit up to 1000 cm^2/V.s of electron carrier mobility (Tuteja and Neethirajan, 2018) while its integration with Au nanoparticles would promote charge transfer among the lattice structure of exfoliated layers. Scan rate dependency studies shown in (Fig. S3 (B)) demonstrates the reversible nature of the redox probe and a linear relationship between the anodic and cathodic peaks with increasing scan rate. The absence of extraneous peaks at higher scan rates (10 mV/s to 200 mV/s) accounts for the stability of BP-AuNC. In addition to CV studies, electrochemical impedance spectroscopy (EIS) was performed to understand the behavior of the synthesized nanocomposite BP-Au using 5 mM $[Fe(CN)_6]^{3-/4-}$ as redox probe. The Nyquist plots and its equivalent circuit (inset) of Fig. S4 represent electron transfer kinetics of different modifications of screen-printed carbon electrodes. The semicircle (high frequency) and line (lower frequency) indicate that the sensing process is governed by electron transfer and diffusion characteristics respectively. The diameter of the semicircle corresponds to the charge transfer resistance (R_{ct}) on the electrode surface, which, as expected is highest for the bare electrode. The Warburg Impedance element and the resistances R_2 and R_3 collectively provide an idea of the solution resistance in the sensing system. A lower resistance was observed on BP modification. Least R_{ct} was observed in the synthesized BP-Au nanocomposite which proves that the electrochemical performance of the synthesized BP-Au nanocomposites is much higher than Au nanoparticles. Hence, a 3 layer deposition of 1 mg/ml BP-Au NC was selected for further studies.

3.2. Optimizing sensor parameters

Working of the sensor was assessed by functionalizing BP-AuNC coated electrode surface with OA-Apt. The redox activity of these electrodes was examined by differential pulse voltammetry (DPV) studies using 5 mM $[Fe(CN)_6]^{3-/4-}$. The aptamer specific to okadaic acid was synthesized with Thiol group (-SH) attached to the 5' end. Thiol-gold bonding is an established mechanism of interaction, where the thiolated biomolecule readily attaches itself to AuNP. This form of chemical adsorption has does not affect the structural or functional properties of the aptamer, thus keeping its sensitivity and selectivity uncompromised (Pensa et al., 2012). The concentration of thiolated aptamer (OA-Apt) deposited on the surface of the electrode was optimized before carrying out redox studies. OA-Apt concentrations ranging from 0.25 μM to 2 μM were immobilized on the surface of modified electrodes in triplicates. Upon aptamer immobilization the WE surface undergoes steric hindrance or blocking, causing a significant reduction in electron transfer kinetics. An apparent current saturation was observed at1 μM shown in (Fig. 3A). Therefore, to avoid higher resistance and lower affinity to aptamer-target binding 1 μM of aptamer was selected for further studies.

Another important factor that contributes to the performance of the sensor is assay time. Optimizing the interaction between OA target and OA-Apt on sensor surface helps in effective sensing. 250 nM of OA was added to the surface of aptamer modified BP-AuNC electrode and allowed to interact. The time span was varied between 5 min–60 min and changes in output current were measured using DPV with 5 mM $[Fe(CN)_6]^{3-/4-}$ as redox indicator (Fig. 3B). The highest peak current was obtained at 5 min and an exponentially decreasing signal was observed with increasing time, finally attaining saturation. The high peak current prior to 30 min could be due to improper binding of OA with OA-Apt, while in the case of longer time periods (60 min) no significant binding occurred. Hence, an incubation time of 30 min was chosen for the final experiment.

3.3. Microfluidic OA aptasensing

The lab – on – chip-based detection system has proven to be a great platform for sensitive biochemical applications. Point-of–care microfluidic devices facilitate low sample consumption, faster and reliable analysis, and high sensitivity. However, utmost care has to be taken in fabrication to avoid deposition of dust and formation of air – pockets, leading to improper adhesion and leaking. In this work, a flexible PDMS based SPCE integrated microfluidic chip was fabricated for the detection of Okadaic acid. A simple Y- channel continuous – flow microfluidic set up was used. The design was specifically made to provide maximum time for incubation of OA Apt, as the sample travels from the inlet to the sensing zone. The width of each channel was set to 200 μm and the sensing zone had a diameter of 4 mm. A zig-zag pattern with corrugation was used to increase mixing effects (Fig. 4B). The microfluidic- SPCE set up was attached to the potentiostat port and the inlets were used to manually inject 50 μL of the sample. This set up is schematically represented in (Fig. 4A). The interaction of OA sample with OA- Apt resulted in a significant reduction of peak current. This change can be related to the repulsion experienced between the negatively charged redox probe $[Fe(CN)_6]^{3-/4-}$ and negatively charged aptamer sequence thus reducing peak current. Hence, for microfluidic aptasensing of OA, optimized parameters of 1 μM of OA- Apt and 30 min incubation time were employed.

Differential pulse voltammetry was used to determine the sensitivity and selectivity of the OA microfluidic biosensor. Aliquots of different concentrations ranging from 50 pM–250 nM were prepared in TE buffer. Form the DPV data shown in (Fig. 5A), it can be understood that the cathodic peak current (8.889 μA) was the highest in the absence of OA (blank). However, when the concentration of OA was increased to 250 nM the cathodic peak current dropped to 2.5 μA (E_{pa} = 0.15 V). The 250 nM concentration Okadaic acid, produced the least amount of current (~0.25 μA) upon interaction with the aptamer. It can be concluded from the study that with increasing concentration of target there is a significant decrease in peak current. This is due to the conformational change occurring in the DNA sequence in the presence of the target molecule. A linear fitting model was developed on the basis of the DPV results where the current was varied against the concentration of OA used. An average of triplicates for each concentration was plotted and the respective standard deviation was represented as error bars (Fig. 5B). is a graphical representation of the obtained current for the various concentrations of Okadaic acid in TE buffer. Various aliquots of OA ranging from 0 to 250 nM were tested with the fabricated biochip and the peak currents were recorded. A good linear relationship was obtained between 10 nM and 250 nM concentration of Okadaic acid, which can be represented by the equation $y = -0.0142x + 6.1139$. The correlation coefficient of the linear range was determined to be $R^2 = 0.9887$. The limit of detection of the biochip was calculated using the standard deviation method, given by the formula (3*σ)/slope. The limit of detection (LOD) of the system was determined to be 8 pM.

A recent study on mouse bioassay revealed that variability in mice strain had a significant effect on its reaction to DSP(Suzuki, 2012). However, with the development of DNA based detection techniques, a more rapid and reliable monitoring system can be achieved. Hence, this study proposes a disposable microfluidic platform as a point of care device for the detection of okadaic acid. The limit of detection of this sensor is comparable to other research works in the same field (Eissa et al., 2013; Rhouati et al., 2013; Hayat et al., 2011). According to food safety standards and guidelines, the minimum dietary limit to cause a significant reaction is 160 μg/kg which is well above the LOD of this sensor. The obtained results demonstrate a proof- of –concept study on the applicability of this sensor in real time.

3.4. Interference studies and real sample analysis

Evaluating cross-reactivity is an important factor in biosensor assessment. It must be ensured that the percentage of false positives in practical applications is kept minimal. To check the selectivity of the OA aptasensor, negative control studies were performed. A concentration (50 nM) of each toxin was prepared in TE buffer and injected into the microchannels. After the incubation time period of 30 min, 100 μL

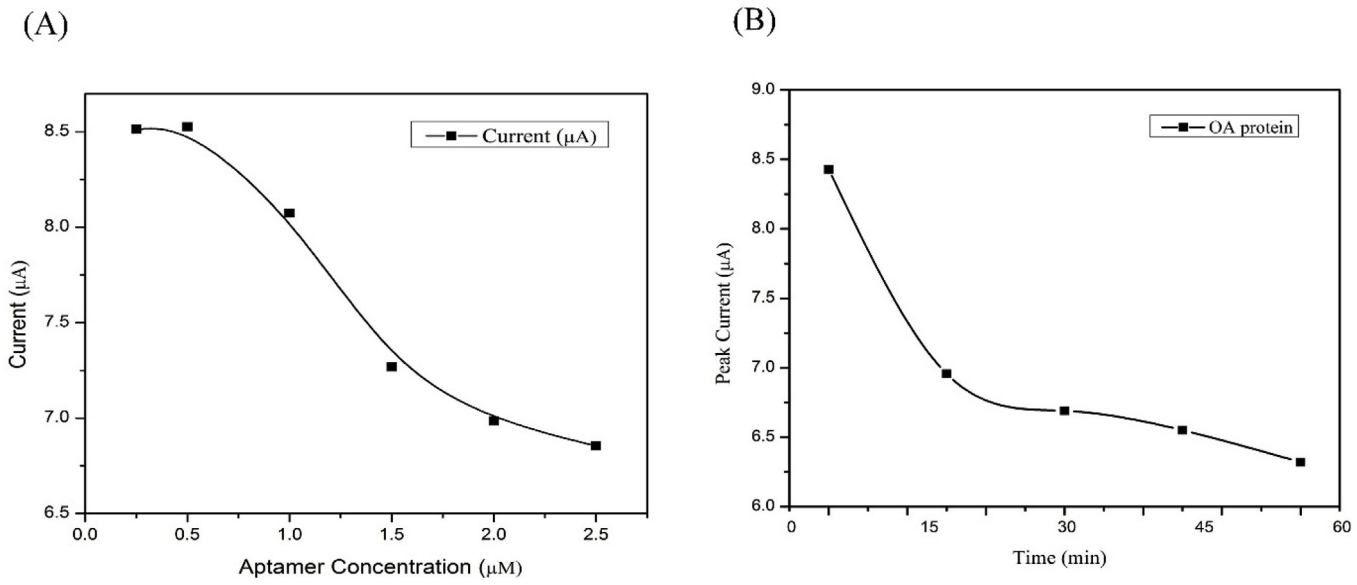

Fig. 3. Optimization of Okadaic Acid aptasensor: (A) Peak currents of DPV signals obtained from various Aptamer concentrations (B) Peak currents of DPV signals of interaction time between OA- Apt and OA target in the presence of 5 mM $[Fe(CN)_6]^{3-/4-}$

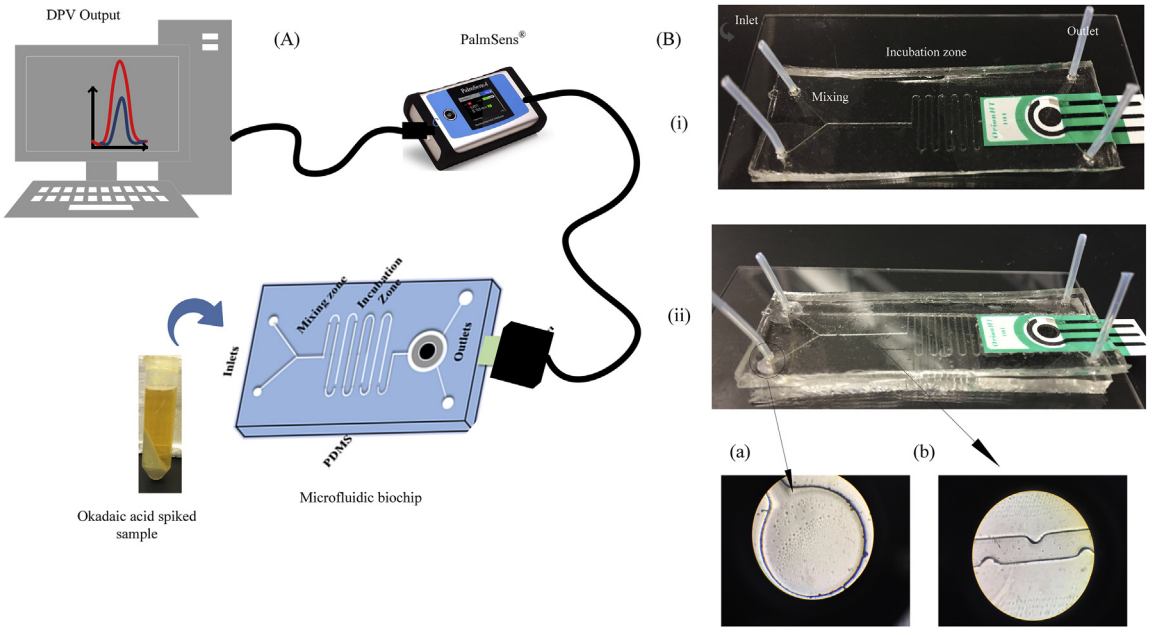

Fig. 4. (A) Schematic of the overall working mechanism of the microfluidic biochip (B) (i) PDMS channels containing inlet, mixing channels, incubation chambers and modified SPCE on a glass substrate (for illustration) and (ii) Prototype of the final sensor (a) Microscopic image of inlet channel (b) Mixing channels having corrugations to facilitate mixing under 50X magnification.

of 5 mM $[Fe(CN)_6]^{3-/4-}$ was used to obtain a DPV response graph. An average of 3 trials (n = 3) was performed for each, to acquire statistical significance. As shown in the graph (Fig. S6), the anodic peak current obtained for all recognition molecules other than OA, was close to blank. This indicates that the interaction between OA-Apt and other biomolecules were non-existent. The average error range for the performed trials was between (6–8%) showing good responsiveness to OA samples. The fabricated sensor did not display any cross-reactivity with brevetoxin or lysozyme.

In addition, fresh mussel samples (uncontaminated) were prepared by steps explained in Section 2.6. The extracts were spiked with a known concentration of OA and injected into the microfluidic channels. DPV analysis of all the different concentrations was run to validate the extent of detection when it comes to shellfish samples. Results discussed in Table 1 explain the extent of recovery for each of the samples examined. The recovery observed was between 2 and 7% for an average of n = 3 replicates. Low error in spiked samples proves the performance of the biosensor in a more complex food matrix. Table S2 compares some of the recent research conducted in the detection of okadaic acid with this study. From these results, it can be concluded that the fabricated microfluidic biosensor can be applied to facilitate real-time monitoring of Okadaic acid levels.

4. Conclusion

This work elucidates the fabrication and working of a microfluidic-based aptasensor for the detection of okadaic acid. An electrochemical approach was preferred for its sensitivity and recovery. Phosphorene,

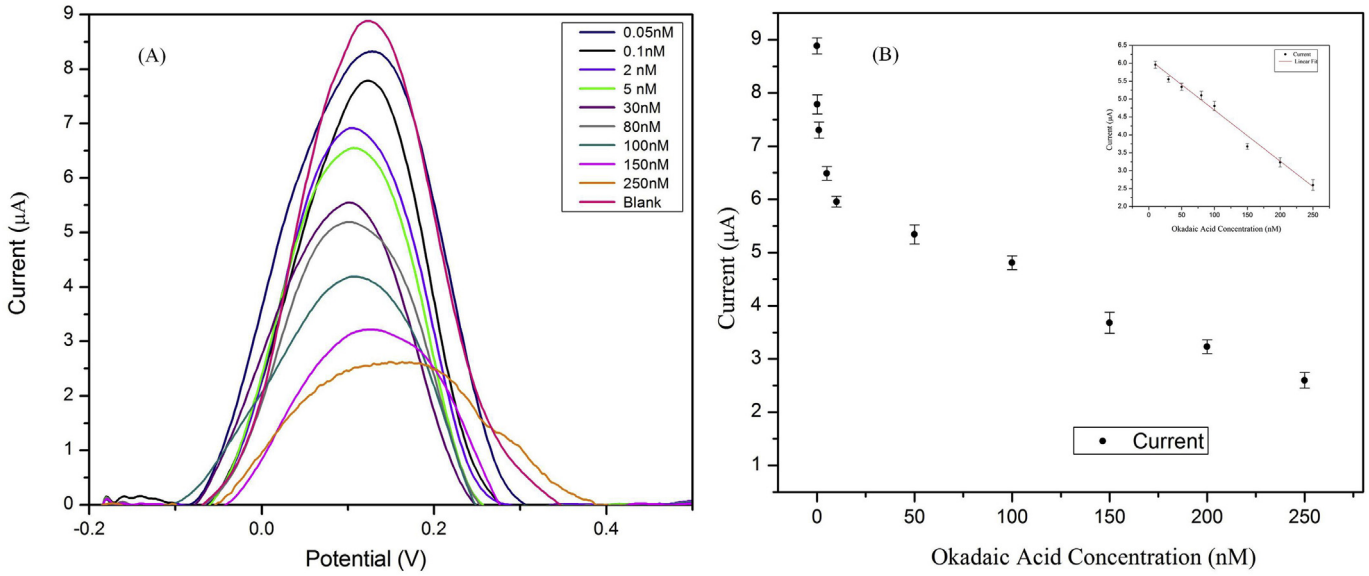

Fig. 5. Okadaic acid aptasensing: (A) DPV signals obtained for various test concentrations of okadaic acid using a ferro-ferri cyanide indicator (B) Peak currents obtained for various concentrations of OA in TE buffer and (Inset) Linear fitting of peak current obtained for OA concentrations (10nM-250nM) having an $R^2 = 0.9887$.

Table 1
Detection of Okadaic acid from spiked mussel extract.

Spiked Concentration (pM)	Detected Concentration (pM)	% Recovery
50	52.18	104.06
500	510.21	102.012
1000	985.25	98.51
2000	1916.79	95.832
5000	4750.53	95

known for its stability and the layered structure was paired with Au nanoparticles for enhanced electroconductivity. This nanocomposite functionalization proved to be effective in anchoring of the aptamer specific to OA without flaking. The aptamer's ability to bind only with incoming OA sample was hypothesized and experimented in a microfluidic setup. The use of a flexible polydimethylsiloxane substrate highly facilitated the integration of the modified SPCE. Sample with various concentrations of OA was administered in a portable fashion and DPV studies were performed in the presence of 5 mM $[Fe(CN)_6]^{3-/4-}$ as a redox indicator. An average assay time of 30 min was required to obtain results for samples with and without OA. The fabricated aptasensor was capable of detecting up to 8 pM of OA sample having a correlation of determination of 0.9887 (R^2). The aptasensor did not show any cross-reactivity with other types of food toxins. It can be concluded that his microfluidic electrochemical aptasensor is not only an easy-to-use, point- of- care device bust has immense scope in being deployed for on-field assay.

CRediT authorship contribution statement

Saipriya Ramalingam: Conceptualization, Data curation, Formal analysis, Investigation, Methodology, Writing - original draft, Writing - review & editing. **Rohit Chand:** Methodology, Investigation. **Chandra B. Singh:** Supervision, Writing - review & editing. **Ashutosh Singh:** Funding acquisition, Resources, Project administration, Supervision, Writing - review & editing.

Acknowledgments

The authors sincerely thank the Natural Sciences and Engineering Research Council of Canada (NSERC) for funding this study (Grant # RGPIN-2017-03975). The authors would also like to acknowledge the OMAFRA- U of G Partnership (Ontario Ministry of Agriculture, Food and Rural Affairs) for funding this study through their Highly Qualified Personnel (HQP) Scholarship Program.

Appendix A. Supplementary data

Supplementary data to this article can be found online at https://doi.org/10.1016/j.bios.2019.03.056.

References

Ahmed, T., Balendhran, S., Karim, M.N., Mayes, E.L.H., Field, M.R., Ramanathan, R., Singh, M., Bansal, V., Sriram, S., Bhaskaran, M., Walia, S., 2017. Degradation of black phosphorus is contingent on UV–blue light exposure. npj 2D Mater. Appl. 1, 18. https://doi.org/10.1038/s41699-017-0023-5.

Bouaïcha, N., Hennion, M.-C., Sandra, P., 1997. Determination of okadaic acid by micellar electrokinetic chromatography with ultraviolet detection. Toxicon 35, 273–281. https://doi.org/10.1016/S0041-0101(96)00069-4.

Cohen, P., Holmes, C.F.B., Tsukitani, Y., 1990. Okadaic acid: a new probe for the study of cellular regulation. Trends Biochem. Sci. 15, 98–102. https://doi.org/10.1016/0968-0004(90)90192-E.

de la Iglesia, P., Gago-Martinez, A., Yasumoto, T., 2007. Advanced studies for the application of high-performance capillary electrophoresis for the analysis of yessotoxin and 45-hydroxyyessotoxin. J. Chromatogr. A 1156, 160–166. https://doi.org/10.1016/J.CHROMA.2006.12.084.

Eissa, S., Ng, A., Siaj, M., Tavares, A.C., Zourob, M., 2013. Selection and identification of DNA aptamers against okadaic acid for biosensing application. Anal. Chem. 85, 11794–11801. https://doi.org/10.1021/ac402220k.

European Food Safety Authority [WWW Document], 2008. https://www.efsa.europa.eu/en/press/news/080131 (accessed 1.4.19).

Hallegraeff, G.M., 1993. A review of harmful algal blooms and their apparent global increase*. Phycologia 32, 79–99. https://doi.org/10.2216/i0031-8884-32-2-79.1.

Hayat, A., Barthelmebs, L., Sassolas, A., Marty, J.L., 2011. An electrochemical immunosensor based on covalent immobilization of okadaic acid onto screen printed carbon electrode via diazotization-coupling reaction. Talanta 85, 513–518. https://doi.org/10.1016/j.talanta.2011.04.034.

Haystead, T.A.J., Sim, A.T.R., Carling, D., Honnor, R.C., Tsukitani, Y., Cohen, P., Hardie, D.G., 1989. Effects of the tumour promoter okadaic acid on intracellular protein phosphorylation and metabolism. Nature 337, 78–81. https://doi.org/10.1038/337078a0.

Huang, H., Xiao, Q., Wang, J., Yu, X.-F., Wang, H., Zhang, H., Chu, P.K., 2017. Black phosphorus: a two-dimensional reductant for in situ nanofabrication. npj 2D Mater. Appl. 1, 20. https://doi.org/10.1038/s41699-017-0022-6.

Ishihara, H., Martin, B.L., Brautigan, D.L., Karaki, H., Ozaki, H., Kato, Y., Fusetani, N., Watabe, S., Hashimoto, K., Uemura, D., Hartshorne, D.J., 1989. Calyculin A and okadaic acid: inhibitors of protein phosphatase activity. Biochem. Biophys. Res. Commun. 159, 871–877. https://doi.org/10.1016/0006-291X(89)92189-X.

Landsberg, J.H., 2002. The effects of harmful algal blooms on aquatic organisms. Rev. Fish. Sci. 10, 113–390. https://doi.org/10.1080/20026491051695.

Liu, H., Neal, A.T., Zhu, Z., Luo, Z., Xu, X., Tománek, D., Ye, P.D., 2014. Phosphorene: an unexplored 2D semiconductor with a high hole mobility. ACS Nano 8, 4033–4041. https://doi.org/10.1021/nn501226z.

Morabito, S., Silvestro, S., Faggio, C., 2018. How the marine biotoxins affect human health. Nat. Prod. Res. 32, 621–631. https://doi.org/10.1080/14786419.2017.1329734.

Pensa, E., Cortés, E., Corthey, G., Carro, P., Vericat, C., Fonticelli, M.H., Benítez, G., Rubert, A.A., Salvarezza, R.C., 2012. The chemistry of the sulfur-gold interface: in search of a unified model. Acc. Chem. Res. 45, 1183–1192. https://doi.org/10.1021/ar200260p.

Ren, X., Lian, P., Xie, D., Yang, Y., Mei, Y., Huang, X., Wang, Z., Yin, X., 2017. Properties, preparation and application of black phosphorus/phosphorene for energy storage: a review. J. Mater. Sci. 52, 10364–10386. https://doi.org/10.1007/s10853-017-1194-3.

Rhouati, A., Hayat, A., Hernandez, D.B., Meraihi, Z., Munoz, R., Marty, J.L., 2013. Development of an automated flow-based electrochemical aptasensor for on-line detection of Ochratoxin A. Sensor. Actuator. B Chem. 176, 1160–1166. https://doi.org/10.1016/j.snb.2012.09.111.

Sassolas, A., Hayat, A., Catanante, G., Marty, J.L., 2013. Detection of the marine toxin okadaic acid: assessing seafood safety. Talanta 105, 306–316. https://doi.org/10.1016/j.talanta.2012.10.049.

Shi, Y., Huang, J.-K., Jin, L., Hsu, Y.-T., Yu, S.F., Li, L.-J., Yang, H.Y., 2013. Selective decoration of Au nanoparticles on monolayer MoS2 single crystals. Sci. Rep. 3, 1839. https://doi.org/10.1038/srep01839.

Stanford, M.G., Rack, P.D., Jariwala, D., 2018. Emerging nanofabrication and quantum confinement techniques for 2D materials beyond graphene. npj 2D Mater. Appl. 2, 20. https://doi.org/10.1038/s41699-018-0065-3.

Stewart, L.D., Hess, P., Connolly, L., Elliott, C.T., 2009. Development and single-laboratory validation of a pseudofunctional biosensor immunoassay for the detection of the okadaic acid group of toxins. Anal. Chem. 81, 10208–10214. https://doi.org/10.1021/ac902084a.

Su, K., Pan, Y., Wan, Z., Zhong, L., Fang, J., Zou, Q., Li, H., Wang, P., 2017. Smartphone-based portable biosensing system using cell viability biosensor for okadaic acid detection. Sensor. Actuator. B Chem. 251, 134–143. https://doi.org/10.1016/j.snb.2017.04.036.

Suzuki, H., 2012. Susceptibility of different mice strains to okadaic acid, a diarrhetic shellfish poisoning toxin. Food Addit. Contam. Part A Chem. Anal. Control. Expo. Risk Assess. 29, 1307–1310. https://doi.org/10.1080/19440049.2012.685892.

Suzuki, H., Okada, Y., 2018. Comparative toxicity of dinophysistoxin-1 and okadaic acid in mice. J. Vet. Med. Sci. 80, 616–619. https://doi.org/10.1292/jvms.17-0377.

Suzuki, T., Miyazono, A., Baba, K., Sugawara, R., Kamiyama, T., 2009. LC–MS/MS analysis of okadaic acid analogues and other lipophilic toxins in single-cell isolates of several Dinophysis species collected in Hokkaido, Japan. Harmful Algae 8, 233–238. https://doi.org/10.1016/J.HAL.2008.06.001.

Teller, C., Shimron, S., Willner, I., 2009. Aptamer-DNAzyme hairpins for amplified biosensing. Anal. Chem. 81, 9114–9119. https://doi.org/10.1021/ac901773b.

Tuteja, S.K., Neethirajan, S., 2018. Exploration of two-dimensional bio-functionalized phosphorene nanosheets (black phosphorous) for label free haptoglobin electro-immunosensing applications. Nanotechnology 29, 135101. https://doi.org/10.1088/1361-6528/aaab15.

Weng, X., Neethirajan, S., 2018. Paper-based microfluidic aptasensor for food safety. J. Food Saf. 38, 1–8. https://doi.org/10.1111/jfs.12412.

Wu, Y.X., Kwon, Y.J., 2016. Aptamers: the “evolution” of SELEX. Methods 106, 21–28. https://doi.org/10.1016/J.YMETH.2016.04.020.

Wu, S., Duan, N., Zhang, H., Wang, Z., 2015. Simultaneous detection of microcysin-LR and okadaic acid using a dual fluorescence resonance energy transfer aptasensor. Anal. Bioanal. Chem. 407, 1303–1312. https://doi.org/10.1007/s00216-014-8378-3.

Wu, X., Xu, Y., Hu, Y., Wu, G., Cheng, H., Yu, Q., Zhang, K., Chen, W., Chen, S., 2018. Microfluidic-spinning construction of black-phosphorus-hybrid microfibres for non-woven fabrics toward a high energy density flexible supercapacitor. Nat. Commun. 9, 4573. https://doi.org/10.1038/s41467-018-06914-7.

Yang, G., Liu, Z., Li, Y., Hou, Y., Fei, X., Su, C., Wang, S., Zhuang, Z., Guo, Z., 2017. Facile synthesis of black phosphorus-Au nanocomposites for enhanced photothermal cancer therapy and surface-enhanced Raman scattering analysis. Biomater. Sci. 5, 2048–2055. https://doi.org/10.1039/c7bm00414a.

Zhang, H., Chhowalla, M., Liu, Z., 2018. 2D nanomaterials: graphene and transition metal dichalcogenides. Chem. Soc. Rev. 47, 3015–3017. https://doi.org/10.1039/c8cs90048e.